EI SEVIER

Contents lists available at ScienceDirect

## Nuclear Inst. and Methods in Physics Research, A

journal homepage: www.elsevier.com/locate/nima



### Full Length Article

# Electrospraying deposition and characterization of potassium chloride targets for nuclear science measurements



S. Dede <sup>a,b</sup>, S.D. Essenmacher <sup>c</sup>, P. Gastis <sup>d</sup>, K.V. Manukyan <sup>a,\*</sup>, S.A. Kuvin <sup>d</sup>, H.Y. Lee <sup>d,\*</sup>, J.M. Roach <sup>e</sup>, P.C. Burns <sup>e,f</sup>, A. Aprahamian <sup>a,e</sup>

- <sup>a</sup> Nuclear Science Laboratory, Department of Physics and Astronomy, University of Notre Dame, Notre Dame, IN 46556, USA
- <sup>b</sup> Cyclotron Institute, Texas A&M University, College Station, TX 77843, USA
- <sup>c</sup> Department of Chemistry, Michigan State University, East Lansing, MI 48824, USA
- <sup>d</sup> Los Alamos National Laboratory, Los Alamos, NM 87545, USA
- e Department of Chemistry and Biochemistry, University of Notre Dame, Notre Dame, IN 46556, USA
- f Department of Civil and Environmental Engineering and Earth Sciences, University of Notre Dame, Notre Dame, IN 46556, USA

#### ARTICLE INFO

# Keywords: Electrospraying deposition Nucellar targets Potassium chloride

#### ABSTRACT

Natural and isotopically enriched KCl targets were prepared using specially formulated KCl solutions, deposited by electrospraying on thin (1.5  $\mu$ m) gold backings, followed by a short annealing in a preheated (350–450 °C) furnace. Various techniques, such as X-ray fluorescence (XRF), scanning electron microscopy (SEM) imaging, and energy-dispersive X-ray spectroscopy (EDS), were used to characterize the produced targets. A white neutron beam at the Los Alamos Neutron Science Center (LANSCE) facility was also used to verify the estimated atomic percentages of the enriched <sup>40</sup>KCl targets. KCl was deposited relatively uniformly as large particles rather than films on the gold surface. This method can be broadly extended to make stable targets that are difficult to produce with other methods and more exotic radioactive targets required for research in fundamental sciences and applications.

#### 1. Introduction

Advances in nuclear science go hand-in-hand with advances in accelerators, detector technologies, and the ability to make robust targets. For most of the history of nuclear science, thin 1– $1000~\mu g/cm^2$  coatings deposited on backings (metal, carbon, or polymer foils) or self-supporting foils were used as targets. Target-making techniques have not significantly advanced in the last five decades and include rolling, vacuum deposition, and electrochemical deposition. These methods were developed in the 1960s and 1970s and were steadily improved to the present day [1–6]. However, challenges remained in making robust targets of radioactive materials. Traditional vacuum deposition methods are typically low in material collection efficiencies (MCE). Targets prepared by electroplating and molecular plating methods contain impurities and are often mechanically unstable during beam exposure.

Polymer-assisted deposition (PAD) is a relatively new method for preparing oxide targets such as  $\rm Eu_2O_3$ ,  $\rm Tm_2O_3$ , and  $\rm HfO_2$ , which are considered analog materials for actinide oxides [7,8]. Aqueous solutions of metal chlorides containing polyethyleneimine are deposited on silicon wafers while rotating at 1500 rpm. Deposited samples are slowly (~5 h) heated to 900 °C, annealed at this temperature, and then cooled at room temperature naturally over the next few hours. The standard

deviation for layer thickness is  $\sim$ 10%. The PAD method can be used in multiple cycles to create thicker films. The MCE for a single application is estimated to be  $\sim$ 33%.

"Drop-on-demand printing" methods involve producing droplets with well-defined volumes and dispensing them on various substrates [9]. The droplets with tunable volumes can be generated by piezo-electrically driven nozzles and deposited on substrates. Water solutions containing radioactive tracers (140 La, 35 S, and 32 P) are used to investigate the deposition process on different backings. The shape and size of the deposited droplets depend on the substrate. This method can potentially provide target preparation procedures with high MCE. However, the printing process must be tailored to produce uniform targets to meet the demand for nuclear science measurements.

Recently, we proposed a novel electrospraying-assisted solution combustion synthesis (SCS) method to prepare  $\rm UO_2$  targets [10] where a reactive solution of uranyl nitrate-acetylacetone-2-methoxyethanol is sprayed onto aluminum backings, followed by immersion in a preheated (350 °C) furnace for 20 min. The self-generated heat during the combustion of the solution layers eliminates the need for extensive and high-temperature post-deposition treatment. Tuning the spraying parameters allows the preparation of  $\rm UO_2$  films with thicknesses varying

E-mail addresses: kmanukya@nd.edu (K.V. Manukyan), hylee@lanl.gov (H.Y. Lee).

<sup>\*</sup> Corresponding authors.

from 10 to  ${\sim}2000~\mu\text{g/cm}^2.$  The high MCE (nearly 100%) makes spraying deposition ideal for fabricating radioactive, rare, and expensive materials.

Here, we report on electrospray deposition of isotopically enriched KCl targets using non-combustible solutions. The targets will be used in cross-section measurements of (n,Z) reactions on <sup>40</sup>K that are relevant to stellar nucleosynthesis and the mechanism responsible for the destruction of  $^{40}$ K in massive stars [11,12]. The half-life of  $^{40}$ K is 1.248  $\times$ 10<sup>9</sup> years and it is one of the naturally occurring radionuclides widely used in radiometric dating. <sup>40</sup>K is also responsible for the radiogenic heating of planets, a process that has been intensively studied in the last decade due to its implication in the evolution of habitable environments in extrasolar planets [13-15]. The method we report here involves spraying specially formulated KCl solutions on gold backings, followed by a short annealing in a preheated (350-450 °C) furnace. Imaging methods show that this process enables the relatively uniform deposition of salt on the gold surface. Electron microscopy imaging also shows that KCl appears primarily as large particles rather than films on the surface of the backings. A white neutron beam at the LANSCE facility was used to verify the estimated atomic percentages of the enriched <sup>40</sup>KCl targets.

#### 2. Experimental procedure

Before electrospraying, thin (1.5  $\mu$ m) gold backings were placed in a furnace, slowly heated to 300 °C, and held at that temperature for 30 min. Visual and optical microscopy show that the electrodeposition of KCl aqueous solutions resulted in non-uniform targets. Therefore, we developed a complex solvent mixture to conduct the deposition of KCl targets. Glycerol is known to dissolve potassium chloride. However, the solution of KCl in glycerol exhibited high viscosity and could not be sprayed. To prepare a KCl solution with optimal viscosity, we dissolved 13.7 mg of natural KCl in 50  $\mu$ l deionized water and sonicated it for 2 min. Then, 0.2552 g of glycerol was added to the solution, sonicated for 5 min, and vortexed for 30 s on a lab mixer. Finally, 0.648 mL of 2-methoxyethanol was added, and the solution was lightly vortexed for 1 min. This solution can be readily sprayed on backings.

We repeated the procedure for 13.7 mg of isotopically enriched  $^{40}\rm KCl$  material (chemical purity level: 97%, isotopic enrichment level: 12.8%) produced by Isoflex USA [12]. The supplied source material was attached to the walls of the shipping glass vial. An attempt to dissolve materials in a water-glycerol mixture was unsuccessful. After adding this solvent mixture, a solid residue floated on the solution's surface. Extended sonication and vortexing steps and more water addition were not helpful, and the solid residue was still observed on the solution's surface. After adding 608  $\mu L$  of 2-methoxyethanol, the solution was passed through a 0.20  $\mu m$  nylon filter to remove the non-dissolved solid. The filtration resulted in  ${\sim}35\%$  solution losses.

Fig. 1 shows a schematic representation of the electrospraying apparatus. The solution of natural KCl was sprayed on the gold surface by applying a 15 kV potential difference between the stainless steel nozzle (0.25 mm inner diameter) and the backings (~7.5 cm from the spraying nozzle), which were heated at 50 °C during the entire process. The flow rate of the solution was 15 µL/h. Spraying was conducted in 90-min segments, followed by an annealing step at 350 °C for 20 min in a furnace. We prepared two natural KCl targets by spraying  ${\sim}90~\mu L$  (n-KCl-1) and  ${\sim}180~\mu L$  (n-KCl-2) solution in four and eight deposition segments, respectively. The final heat treatment of targets included annealing at 350 °C for 5 min, then ramping to 450 °C within 10 min and annealing at 450 °C for 30 min. The concentration and final volume of the  $^{40}$  KCl solution were not precisely determined due to the solution losses during the filtration step. Subsequently, the number of deposition segments for the 40 KCl solution were reduced compared to the natural KCl targets. The electrospraying parameters were the same as for the previous targets. We prepared two targets (40KCl-1 and <sup>40</sup>KCl-2) with four and one target (<sup>40</sup>KCl-3) with three deposition

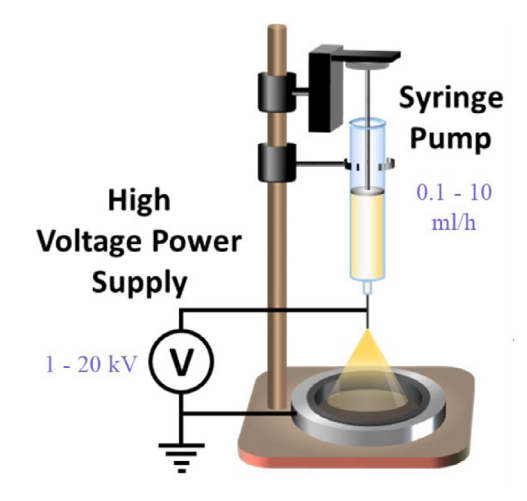


Fig. 1. Schematics of the electrospraying setup.

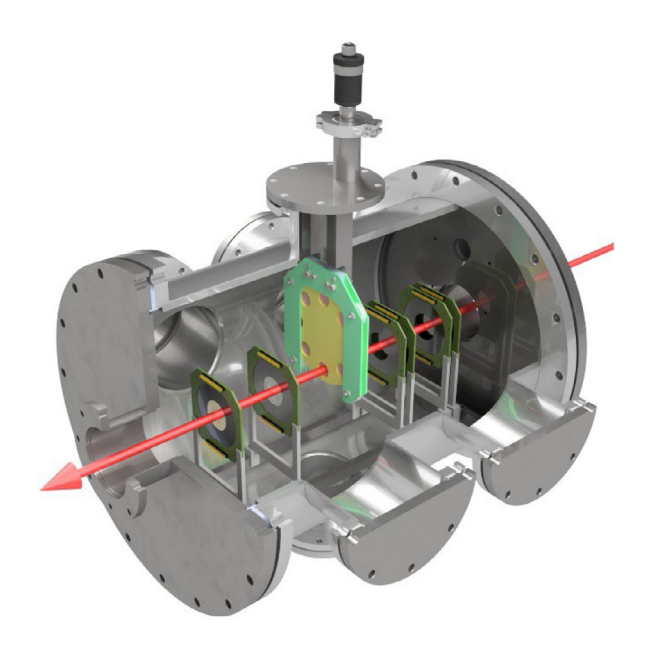


Fig. 2. Schematics of the LENZ experimental chamber.

segments, respectively. All targets were mounted on aluminum frames with 25 mm in diameter openings using conductive cement.

An Orbis X-ray fluorescence (XRF) analyzer (EDAX) with an Rh Xray tube, poly-capillary optics, and an 80 mm2 Silicon drift detector (SDD) was utilized to characterize the targets. The elemental composition and the overall uniformity of the targets were determined, with a collimated X-ray beam (2 mm diameter) obtained by the tube operating at 40 kV and 400  $\mu A$ . The microstructure of the targets was examined with field-emission scanning electron microscopy (SEM) using a Helios NanoLab 600 (Thermo) microscope. Energy-dispersive Xray spectroscopy (EDS, Bruker) using a SDD detector (energy resolution of 130 eV at 5.9 keV) was employed to analyze the elemental compositions of the targets. A supplementary analysis of the elemental and isotopic compositions of K and Cl was performed using the Low-Energy (n,Z) (LENZ) [16] instrument at the Los Alamos Neutron Science Center (LANSCE) [17]. This analysis involved the measurement of proton yields from the  $^{39}{\rm K(n,~p_0)^{39}Ar}$  and  $^{35}{\rm Cl(n,~p_0)^{35}S}$  reaction channels as described in Section 3. A rendering of the LENZ experimental chamber is shown in Fig. 2 [18], and a schematic of outgoing reactions is shown in Fig. 2. of Ref. [16]. The current targets were fabricated on thin gold backings, allowing detectors to be placed upstream and downstream

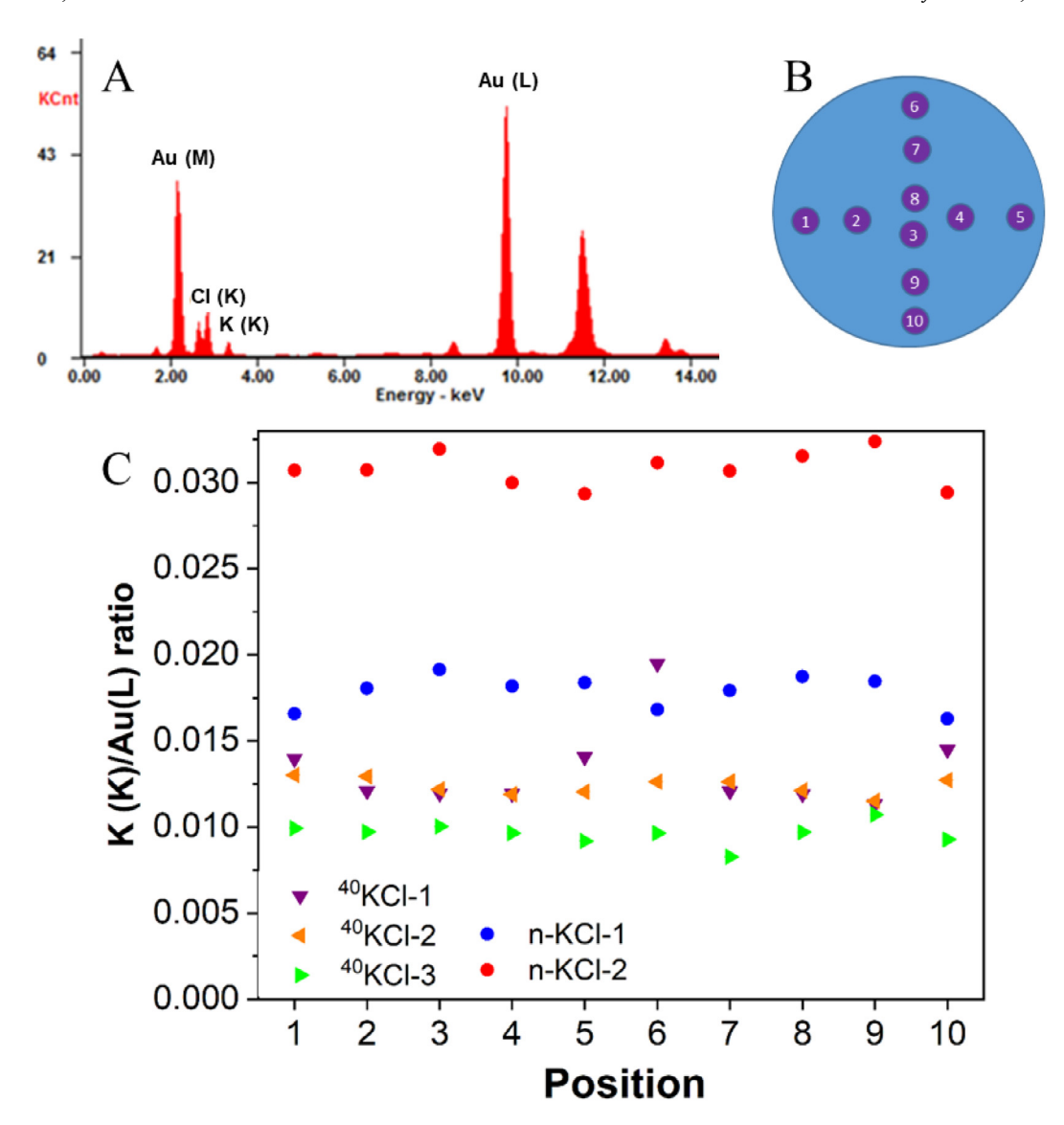


Fig. 3. A typical XRF spectrum of a KCl/Au target (A), schematic representation of XRF measurements (B). The purple circles are the approximate locations of probed areas. K(K)/Au(L) peak ratio for different targets (C). The uncertainties are smaller than the data points on panel C.

of the target to cover both forward and backward angles. The proton yields from the nuclear reactions were extracted, and the estimated atomic percentages of the enriched  $^{40}$ KCl targets were calculated.

### 3. Results and discussions

Fig. 3 summarizes the XRF analysis results for n-KCl and  $^{40}$ KCl. A representative XRF spectrum of a target shows that the Cl(K) characteristic line (2.31 keV) overlaps with one of the Au  $\rm M_{\alpha}$  line (2.31 keV) series, making the determination of target uniformity by the chloride peak uncertain (Fig. 3A). Therefore, to probe the uniformity, we compare the K(K) (3.31 keV) and Au L (9.71 keV) peaks in ten different positions on targets (Fig. 3B). K(K)/Au(L) peak ratios show that natural KCl is mostly uniformly deposited on the Au backing (Fig. 3C).

The conditions for preparing the n-KCl-2,  $^{40}$ KCl-1, and  $^{40}$ KCl-2 targets were similar. However, K(K)/Au(L) ratios for isotopically enriched targets are lower than the ratio for n-KCl-2 (Fig. 3C). This difference may be explained by the reduced concentration of  $^{40}$ KCl in the spraying solution due to the encountered solution preparation difficulties. An area (position 6) for the  $^{40}$ KCl-1 target exhibits a higher potassium concentration. This non-uniform area is due to the deposition of larger

droplets at the end of the process. The K(K)/Au(L) ratio for  $^{40}KCl-3$  is lower than the two enriched targets.

SEM images show that both n-KCl-2 (Fig. 4A) and  $^{40}$ KCl-2 (Fig. 4B) targets have a relatively uniform distribution of material with a brighter contrast on darker backing. EDS spectra acquired from large (2000  $\times$  1500  $\mu m$ ) areas for both targets exhibit Au(M), Cl(K), and K(K) characteristic X-ray lines along with oxygen (0.52 keV) and adventitious carbon (0.27 keV) peaks. In addition to these peaks, the EDS spectrum of the  $^{40}$ KCl-2 target exhibits a Na(K) characteristic line with 1.04 keV energy.

We also conducted high-resolution SEM imaging and local EDS analysis of n-KCl-2 (Fig. 5A) and  $^{40}$ KCl-2 (Fig. 5B). Two types of KCl are observed for both targets: particles (10–20 µm) with darker contrast and dendritic-type crystals (lighter contrast). Local EDS analysis shows (Fig. 5) that both structures exhibit similar elemental composition. EDS spectra (Fig. 5) acquired from the dendrites exhibit intense gold peaks compared to the particles, suggesting that dendrites are much thinner than the particles. Therefore, the contrast differences between large particles and dendrites are related to their sizes. Closer imaging shows that dendrites always originate from larger crystals. Such microstructure suggests that the large particles formed first, then dendrites grew from nucleation sites on particles during a secondary growth process.

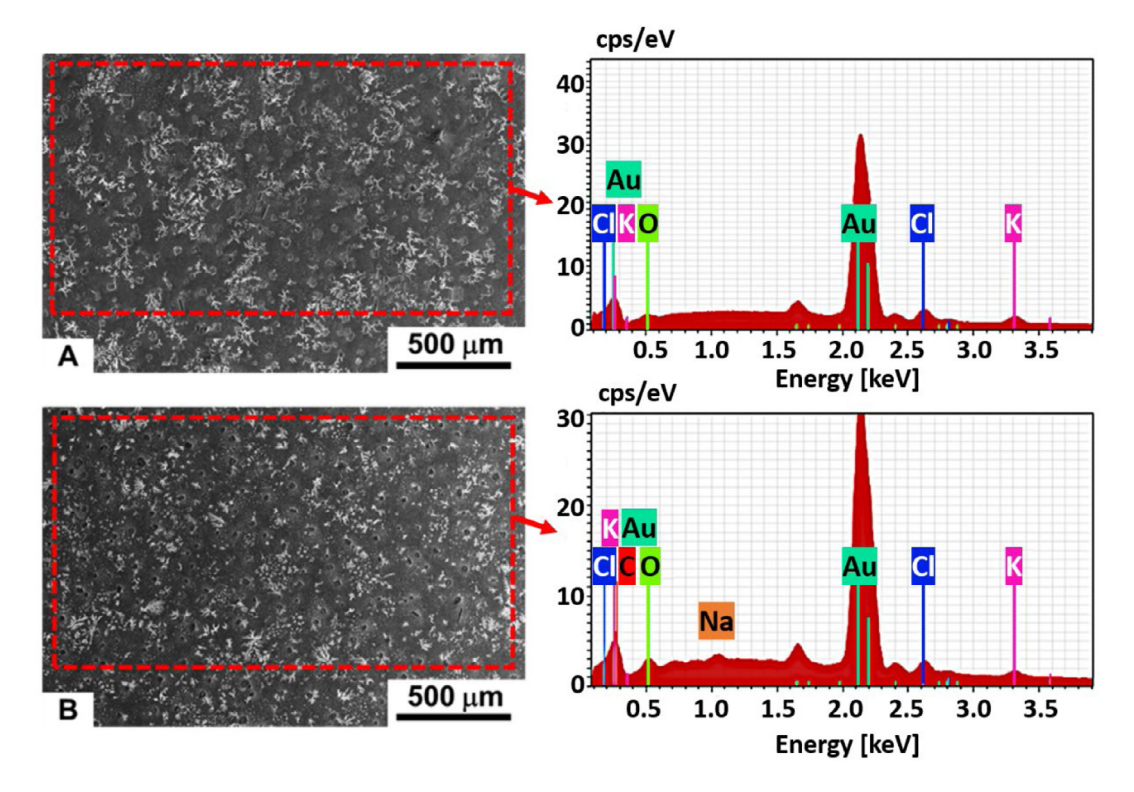


Fig. 4. SEM images and EDS spectra of n-KCl-2 (A) and 40 KCl-2 (B) targets.

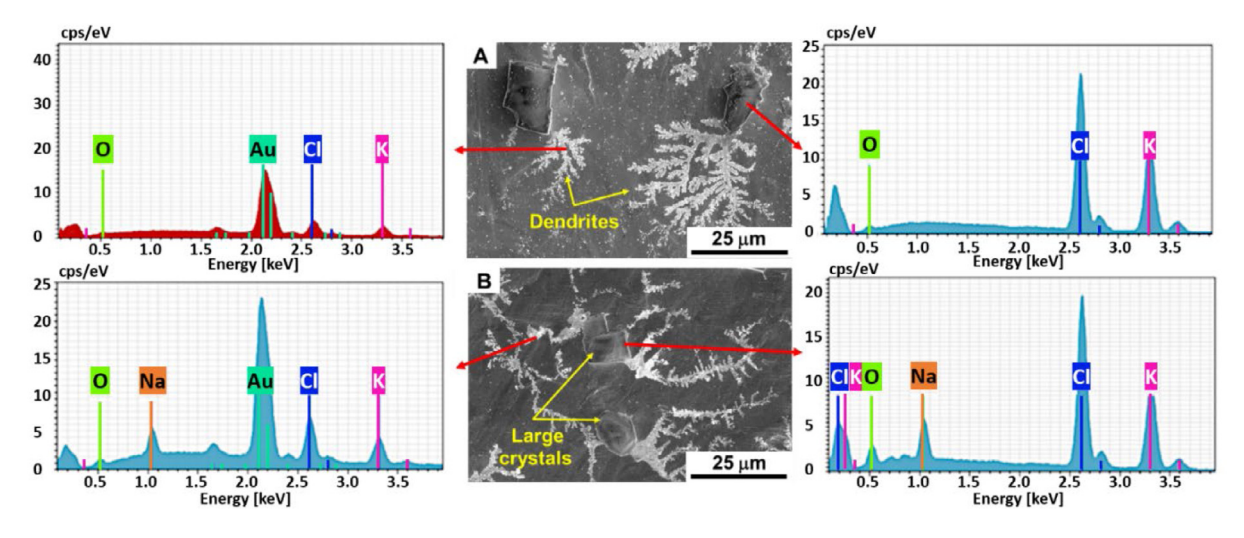


Fig. 5. High-resolution SEM images and local EDS spectra of large particles (right) and dendritic crystals (left) of the n-KCl-2 (A) and <sup>40</sup>KCl-2 (B) targets.

We can assume that some glycerol remains on the targets during the preliminary annealing segments (350 °C) due to its relatively high boiling point (290 °C). Spontaneous growth of dendrites could be triggered upon cooling glycerol residues saturated with KCl.

In addition to the SEM images, 2D and 3D optical images were also taken using a Keyence VK-X3100 laser confocal microscope. The 3D image in Fig. 6A was obtained using the focus variation method. This method involves taking 2D cross-sectional images of the x-y plane as the optical lens moves along the z-axis. At each point on the z-axis, the in-focus features of the topography of the surface are captured. These slices are then "stacked" to produce a 3D image [19]. Corrections were performed after constructing a 3D image to account for the curvature observed in the Au foil backing. The images were taken with a 10x magnification optical lens with a  $360^\circ$  light ring. The light ring

increases the aperture of the illumination, which helps improve the resolution of materials that tend to scatter light easily or have sharp edges. [19]

The results for the  $^{40}$  KCl-3 sample in Fig. 6A and B, confirm the particle (10–20  $\mu m)$  and dendritic-type crystals we observed using SEM. Despite the seemingly non-uniform deposition of the KCl crystals due to clusters appearing in the top left and bottom right of the 3D image, most deposited crystals have heights of approximately 10  $\mu m$  and are thus uniform in height (Fig. 6A). The dendrites originating from the larger particles can be seen in the form of a reddish hue on 2D optical image (Fig. 6B).

The EDS spectrum taken from the large particles of the n-KCl-2 target shows K (49.3 at.%), Cl (48.4 at.%), and O (2.3 at.%) composition. The composition of large particles for the  $^{40}$ KCl-2 target is K (40.1%),

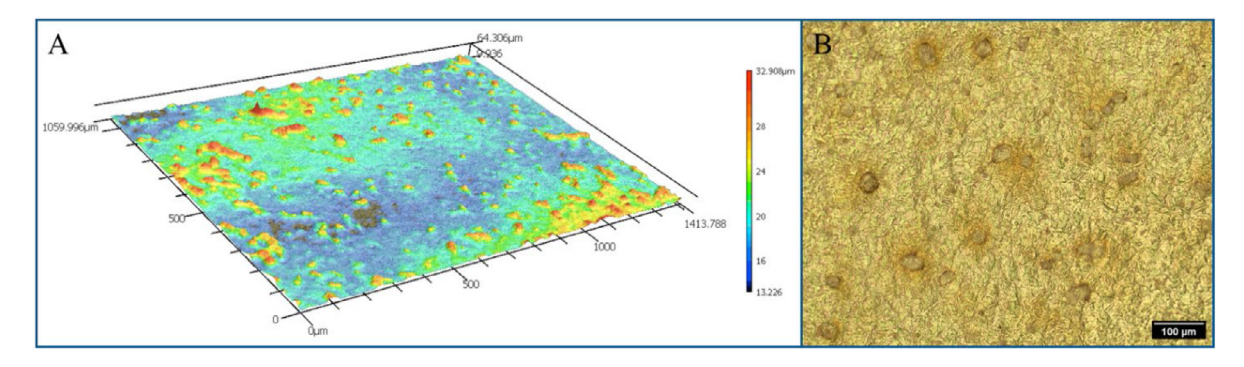


Fig. 6. 3D image of the 40 KCl-3 target using the focus variation method (A) and 2D optical image. (B).

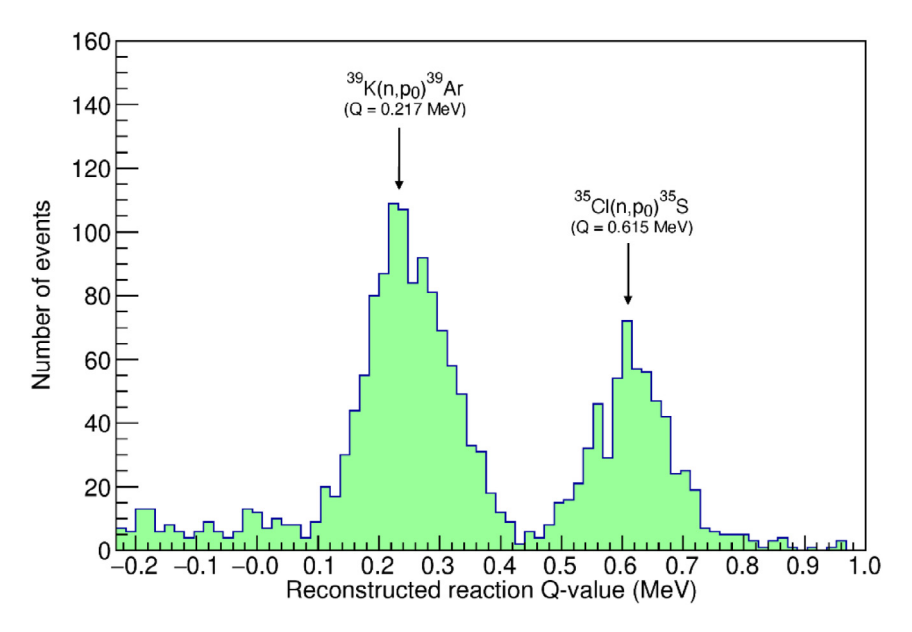


Fig. 7. Reconstructed Q-values for the (n,p) reactions of interest. The plot displays events from the natural KCl target for  $3.0 < E_{neut} < 3.5$  MeV.

 $\begin{array}{ll} \textbf{Table 1} \\ \textbf{Chemical admixtures with more than 25 ppm concentration.} \end{array}$ 

Element	Na	В	Si	P	Rb	Mg	Br	Ca	Fe	Sr	Ва
Content (ppm)	25 000	2900	1200	240	240	130	70	<50	<50	30	26

Cl (43.1%), Na (5.6%), and O (11.2%). The differences suggest that the source material contained sodium contamination in two forms: NaCl and an unknown Na compound with light elements (O, C, and/or H). Table 1 has a list with the admixtures found in the  $^{40}\rm KCl$  targets based on the certificate analysis of the sample from Isoflex.

To confirm the estimated atomic percentages of the enriched  $^{40}\text{KCl}$  targets extracted from the EDS analysis, a test measurement with a white neutron beam at LANSCE was conducted. In this measurement, the natural n-KCl-1 and enriched  $^{40}\text{KCl-2}$  samples were irradiated with fast neutrons, while the number of emitted protons from the  $^{39}\text{K(n,}$   $p_0)^{39}\text{Ar}$  and  $^{35}\text{Cl(n,}$   $p_0)^{35}\text{S}$  reaction channels were measured using the LENZ instrument. The proton yields from the nuclear reactions were extracted by integrating the number of events in the corresponding Q-value spectra, as shown in Fig. 7. The events from  $^{39}\text{K(n,}$   $p_0)$  and  $^{35}\text{Cl(n,}$   $p_0)$  channels appear as individual peaks separated by  ${\sim}400$  keV. The integrals of those peaks at the various incident neutron energies corresponding to the proton  $N_{39\text{K}}$  and  $N_{35\text{Cl}}$  yields are inserted in Eq. (1).

Fig. 8 displays the test measurement results for six incident neutron energies. The cross-section ratio for each incident neutron energy was

calculated as:

$$\frac{\sigma_{39K}}{\sigma_{35Cl}} = \frac{A_{Cl} \times I_{35Cl} \times N_{39K}}{A_{K} \times I_{39K} \times N_{35Cl}}$$
 (1)

where,  $\sigma$  is the (n,  $p_0$ ) partial cross-section, A is the atomic percentage of each element, I is the isotopic ratio, and N is the number of detected protons from each reaction channel.

For the n-KCl-1, the atomic and isotopic abundances of interest were  $A_{Cl} = AK = 0.5$ ,  $I_{35Cl} = 0.7577(10)$ , and  $I_{39K} = 0.933$ , while for the enriched  $^{40}$  KCl-2 target the abundances were  $A_{\rm Cl}$  = 0.4308(215),  $A_K = 0.4012(201)$ ,  $I_{35Cl} = 0.7577(10)$ , and  $I_{39K} = 0.569(22)$ . The isotopic abundance of  $I_{39K}$  in the enriched target was obtained from the certificate analysis of the sample from Isoflex [12] and is presented in Table 2. The isotopic abundance of I<sub>35Cl</sub>was obtained from the NuDat 3.0 library [20]. The atomic abundances for the natural and the enriched targets were determined by the EDS analysis assuming an error of 5%. The ratios of the cross-sections in the enriched and natural targets were found to agree, with their differences being well within the  $\sim$ 5% uncertainty of the EDS analysis and the  $\sim$ 3% statistical uncertainty of the proton yield measurements. The results confirm that the expected values of the atomic percentages A<sub>Cl</sub> and A<sub>K</sub> of the enriched target inserted in Eq. (1) are accurate and validate the characterization method of the sample.

#### 4. Conclusions

We have demonstrated that electrospraying is a viable method for the preparation of natural and isotopically enriched KCl targets

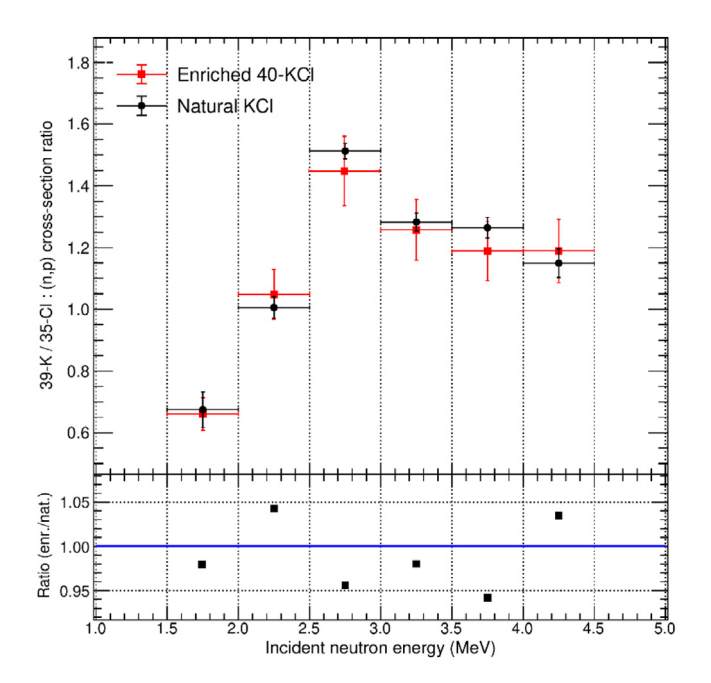


**Fig. 8.** Ratios of partial cross-sections of  $^{39}$ K(n,  $p_0$ ) and  $^{35}$ Cl(n,  $p_0$ ) reaction channels in the enriched and natural KCl targets (upper panel). Deviations of the cross-section ratios between the enriched and natural targets (lower panel).

Table 2
Isotopic distribution.

Isotope	K-39	K-40	K-41
Content (%)	$56.9 \pm 2.2$	$12.8\pm0.5$	30.3
Q-value (n,p) (keV)	$217 \pm 5$	$2286.75 \pm 6$	$-1709.7 \pm 3$

for nuclear science measurements. The reported procedure enables the preparation of uniform targets of radionuclides available only in quantities of a few milligrams. The multiple deposition cycles followed by short annealing steps enable the production of targets with a tunable amount of KCl on the backings. The deposited material primarily forms relatively large, isolated particles rather than thin films on the gold backings, due to the nature of the starting material and surface properties of the substrate. This method can be broadly extended to make stable targets that are difficult to produce with other methods, as well as more exotic radioactive targets required for research in fundamental sciences and applications.

#### **Declaration of competing interest**

The authors declare that they have no known competing financial interests or personal relationships that could have appeared to influence the work reported in this paper.

#### Data availability

No data was used for the research described in the article.

#### Acknowledgments

The work was performed with financial support from the U.S. Department of Energy's (DOE) National Nuclear Security Administration, USA (NNSA, Grants # DE-NA0003913, and NA0004093) and

U.S. National Science Foundation (NSF, PHY 2011890). This research benefited from the use of LANSCE, which is supported by the NNSA, USA, under Contract No. 89233218CNA000001. The authors also acknowledge Notre Dame Center for Environmental Science & Technology (CEST) and Integrated Imaging Facility (NDIIF) for instrumentation usage.

#### References

- S. Clifford, X. Guo-ji, C. Ingelbrecht, M.J. Pomeroy, Processes for the production of ultra-pure metals from oxide and their cold rolling to ultra-thin foils for use as targets and as reference materials, Nucl. Instrum. Methods Phys. Res. A 480 (2002) 29–35, http://dx.doi.org/10.1016/S0168-9002(01)02043-5.
- A. Stolarz, Target preparation for research with charged projectiles, J. Radioanal.
   Nucl. Chem. 299 (2014) 913–931, http://dx.doi.org/10.1007/s10967-013-2652-2
- [3] J.M. Heagney, Preparation of isotopic accelerator targets n.d., 102, 451-5.
- [4] N. Trautmann, H. Folger, Preparation of actinide targets by electrodeposition, Nucl. Inst. Methods Phys. Res. A 282 (1989) 102–106, http://dx.doi.org/10. 1016/0168-9002(89)90117-4.
- [5] S. Sadi, A. Paulenova, P.R. Watson, W. Lovel, Growth and surface morphology of uranium films during molecular plating, Nucl. Inst. Methods Phys. Res. A 655 (2011) 80–84, http://dx.doi.org/10.1016/j.nima.2011.06.025.
- [6] J.P. Greene, I. Ahmad, Molecular plating of actinides on thin backings, Nucl. Inst. Methods Phys. Res. A 590 (2008) 131–133, http://dx.doi.org/10.1016/j. nima.2008.02.076.
- [7] M.N. Ali, M.A. Garcia, T. Parsons-Moss, H. Nitsche, Polymer-assisted deposition of homogeneous metal oxide films to produce nuclear targets, Nat. Protoc. 5 (2010) 1440–1446, http://dx.doi.org/10.1038/nprot.2010.105.
- [8] M.A. Garcia, M.N. Ali, T. Parsons-Moss, P.D. Ashby, H. Nitsche, Metal oxide films produced by polymer-assisted deposition (PAD) for nuclear science applications, Thin Solid Films 516 (2008) 6261–6265, http://dx.doi.org/10.1016/j.tsf.2007. 11.127.
- [9] R. Haas, S. Lohse, C. Düllmann, K. Eberhardt, C. Mokry, J. Runke, Development and characterization of a drop-on-demand inkjet printing system for nuclear target fabrication, Journal (2017) 874, http://dx.doi.org/10.1016/j.nima.2017. 08.027.
- [10] S. Dede, K.V. Manukyan, J.M. Roach, A. Majumdar, P.C. Burns, A. Aprahamian, Irradiation-induced amorphization of UO2 films prepared by spraying-assisted combustion synthesis, Appl. Surf. Sci. 603 (2022) 154437, http://dx.doi.org/10. 1016/j.apsusc.2022.154437.
- [11] S.E. Woosley, A. Heger, T.A. Weaver, The evolution and explosion of massive stars, Rev. Modern Phys. 74 (2002) 1015, http://dx.doi.org/10.1103/RevModPhys.74.1015.
- [12] P. Gastis, G. Perdikakis, J. Dissanayake, P. Tsintari, I. Sultana, C.R. Brune, et al., Constraining the destruction rate of <sup>4</sup>0K in stellar nucleosynthesis through the study of the <sup>4</sup>0Ar(p, n)<sup>40</sup>K reaction, Phys. Rev. C 101 (2020) 55805, http://dx.doi.org/10.1103/PhysRevC.101.055805.
- [13] F. Nimmo, J. Primack, S.M. Faber, E. Ramirez-Ruiz, M. Safarzadeh, Radiogenic heating and its influence on rocky planet dynamos and habitability, Astrophys. J. Lett. 903 (2020) L37, http://dx.doi.org/10.3847/2041-8213/ABC251.
- [14] B.J. Foley, A.J. Smye, Carbon Cycling and Habitability of Earth-Sized Stagnant Lid Planets. https://HomeLiebertpubCom/Ast 18 (2018) 873–96. http://dx.doi. org/10.1089/AST.2017.1695.
- [15] E.A. Frank, B.S. Meyer, S.J. Mojzsis, E.A. Frank, B.S. Meyer, S.J. Mojzsis, A radiogenic heating evolution model for cosmochemically earth-like exoplanets, Icar 243 (2014) 274–286, http://dx.doi.org/10.1016/J.ICARUS.2014.08.031.
- [16] S.A. Kuvin, H.Y. Lee, T. Kawano, B. Digiovine, A. Georgiadou, C. Vermeulen, et al., Nonstatistical fluctuations in the Cl 35 (n, p) S 35 reaction cross section at fast-neutron energies from 0.6 to 6 MeV, Phys. Rev. C (2020) 102, http://dx.doi.org/10.1103/PHYSREVC.102.024623.
- [17] P.W. Lisowski, C.D. Bowman, G.J. Russell, S.A. Wender, The Los Alamos National Laboratory Spallation Neutron Sources. http://dx.doi.org/10.13182/NSE90-A27471 106 (2017) 208–18. http://dx.doi.org/10.13182/NSE90-A27471.
- [18] H.I. Kim, H.Y. Lee, T. Kawano, A. Georgiadou, S.A. Kuvin, L. Zavorka, et al., New evaluation on angular distributions and energy spectra for neutron-induced charged-particle measurements, Nucl. Inst. Methods Phys. Res. A (2020) 963, http://dx.doi.org/10.1016/J.NIMA.2020.163699.
- [19] F. Helmli, Focus variation instruments, in: Leach R. (Ed.), Opt. Meas. Surf. Topogr., Springer Berlin Heidelberg, Berlin, Heidelberg, 2011, pp. 131–166, http://dx.doi.org/10.1007/978-3-642-12012-1\_7.
- [20] Nudat 3, 2023, n. d., https://www.nndc.bnl.gov/nudat3/ (accessed April 2, 2023).